

# RSC Advances



This is an *Accepted Manuscript*, which has been through the Royal Society of Chemistry peer review process and has been accepted for publication.

*Accepted Manuscripts* are published online shortly after acceptance, before technical editing, formatting and proof reading. Using this free service, authors can make their results available to the community, in citable form, before we publish the edited article. This *Accepted Manuscript* will be replaced by the edited, formatted and paginated article as soon as this is available.

You can find more information about *Accepted Manuscripts* in the [Information for Authors](#).

Please note that technical editing may introduce minor changes to the text and/or graphics, which may alter content. The journal's standard [Terms & Conditions](#) and the [Ethical guidelines](#) still apply. In no event shall the Royal Society of Chemistry be held responsible for any errors or omissions in this *Accepted Manuscript* or any consequences arising from the use of any information it contains.



Journal Name

ARTICLE

Received 00th January 20xx,  
Accepted 00th January 20xx  
DOI: 10.1039/x0xx00000x  
www.rsc.org/

## Towards the development of eco-friendly disposable polymers: ZnO-initiated thermal and hydrolytic degradation in Poly (L-lactide)/ZnO nanocomposites

E. Lizundia<sup>a</sup>, L. Ruiz-Rubio<sup>a</sup>, J. L. Vilas<sup>a,b</sup> and L. M. León<sup>a,b</sup>

In this work Poly(L-lactide)/ZnO nanocomposites with homogeneously distributed nanoparticles have been fabricated by solvent-precipitation method. Obtained nanocomposites have been submitted to thermal and hydrolytic degradation processes in order to elucidate the catalytic effect of ZnO nanoparticles. The resulting degradation products from the thermally-initiated catalysis have been identified by Fourier Transform Infrared Spectroscopy (FTIR). It has been found that the presence of ZnO gives rise to a 65-fold increase in the formation of CO<sub>2</sub> in comparison to acetaldehyde. FTIR results of hydrolytically degraded nanocomposites show an increased amount of carboxylic acid groups as ZnO concentration raises, while the C=O stretching band splitting denoted larger crystalline regions as degradation proceeds. Obtained results are explained from the viewpoint of lattice oxygen vacancies in ZnO. Upon thermodegradation nanoparticles initiate unzipping depolymerization/intermolecular transesterification reactions in PLLA, while during hydrolytic degradation H<sub>2</sub>O is dissociated on oxygen vacancy sites, giving hydroxyl groups that initiate the hydrolysis of ester bonds, and thus reducing PLLA to soluble monomers. Obtained findings are expected to allow the development of eco-friendly disposable polymeric waste by opening new possibilities in the use of naturally-available materials as efficient catalyst for the feedstock recycling of biopolymers by common chemical processes.

### Introduction

Nowadays there is an increasing interest from both academia and private industry towards the development of a sustainable society. In this trend of obtaining sustainable materials, especially interesting is the development of biopolymer-based parts to be used in packaging industry, where the use of non-biodegradable materials for short-term use applications is very widespread. In this sense, biodegradable polymers such as poly (L-lactide) (PLLA) have been gaining both scientific and commercial significance due to their inherent physicochemical characteristics and their renewable character.<sup>1,2</sup> Besides fulfilling the requirements of the traditionally available thermoplastics such as polyethylene terephthalate (PET), polystyrene (PS) and polypropylene (PP), their economically feasible industrial production makes polylactides interesting candidates to replace current petroleum-based plastics.<sup>3,4</sup>

At the present time, the feedstock recycling of biopolymers by common chemical processes remains insufficiently explored and is still open to debate. Thereby, it results highly desirable to develop industrial processes in which the plastic recycling would be carried out at low cost and in a controllable way. In this framework, Fan et al. have shown that alkali earth metal oxides such as calcium oxide (CaO) and magnesium oxide (MgO) selectively produce L,L-lactide and lowered thermal degradation temperature, which would serve

for the feed stock recycling of PLLA.<sup>5</sup> In a similar work, Motoyama et al. found that the catalytic activity of MgO markedly increases in presence of smaller particles because of the increase in the catalytic surface area.<sup>6</sup> In view to those results, in this work we use more economically feasible catalyst particles as a cost-effective approach to reduce PLLA and in that way develop eco-friendly disposable materials. Among all the available materials, zinc oxide nanoparticles (ZnO) are of special interest since they present higher catalytic efficiency in regard to other materials in both aqueous and air media.<sup>7-9</sup> Since catalytic reactions usually take place at the particle surfaces, the use of large surface area nanorods is desirable for enhancing the activity of zinc oxide.<sup>10</sup> At the same time, by using biocompatible zinc oxide nanoparticles UV-absorbing films with high visible transparency would be achieved,<sup>11</sup> preventing food photodegradation when PLLA is used as packaging material.<sup>12-15</sup>

Spectroscopic and non-destructive techniques such as Fourier Transform Infrared Spectroscopy (FTIR) are of key relevance to understand degradative processes of polymers since they allow identifying compounds while enable the determination of crystalline phases when intermolecular interactions take place.<sup>16</sup> In this sense, the degradation mechanism induced by the presence of ZnO nanoparticles could be identified by the FTIR analysis of the evolved gases resulting from the chain cleavage of the PLLA/ZnO nanocomposites. Moreover, the analysis of the carbonyl (C=O) stretching band, which remains almost uncoupled from the vibrational modes of the backbone chain,<sup>17</sup> would provide information about the conformational changes occurring during the hydrolytic degradation of PLLA-based materials.

ZnO nanoparticles have been previously used to improve the photocatalytic activity of thermoplastic polymers such as polypropylene (PP).<sup>18</sup> However, to the best of our knowledge, no

<sup>a</sup> Macromolecular Chemistry Research Group (LABQUIMAC). Dept. of Physical Chemistry. Faculty of Science and Technology. University of the Basque Country (UPV/EHU), Spain.

<sup>b</sup> Basque Center for Materials, Applications and Nanostructures (BCMaterials), Parque Tecnológico de Bizkaia, Ed. 500, Derio 48160, Spain.  
E-mail: erlantz.lizundia@ehu.eus

† Electronic Supplementary Information (ESI) available: See DOI: 10.1039/x0xx00000x

previous work have been devoted to the systematic study of the reactions occurring in both thermally and hydrolytically catalyzed reactions in biopolymers in presence of ZnO. Thereby, in this work we attempt to elucidate how the presence of ZnO nanoparticles affects the resulting catalytic processes of PLLA, which would help the packaging industry to develop new disposable materials. FTIR has been carried out to identify thermodegradation compounds together with the conformational changes occurring during the hydrolytic degradation of PLLA-based materials. According to the 12 Principles of Green Chemistry,<sup>19</sup> the development of renewable PLLA-based nanocomposites with well-dispersed ZnO nanoparticles would open new insights towards the development of eco-friendly disposable polymeric waste.

## Experimental

### Materials and sample preparation

PLLA with a number-average molecular weight ( $M_n$ ) of 100,000g/mol and a polydispersity index ( $M_w/M_n$ ) of 1.85 (see molecular weight distribution in the Supplementary data, Fig S1) has been supplied by Purac Biochem. Phosphate buffered saline (PBS) tablets were supplied by Sigma Aldrich, chloroform (reagent  $\geq 99.8\%$ ) was purchased from LabScan and methanol (reagent  $\geq 99.5\%$ ) was purchased by Panreac. Zinc oxide (ZnO) nanoparticles, with a purity of  $\geq 99.5\%$  according to obtained X-ray diffraction pattern (Fig 1a), have been kindly purchased by L'Urederra technological centre (Spain).

Samples have been prepared by solvent-precipitation followed by compression moulding. Firstly, ZnO nanoparticles were homogeneously dispersed in chloroform ( $\text{CHCl}_3$ ) via mild-sonication (20% output for 1 minute) in a Vibra-Cell™ CV 334 ultrasonic processor. Finely dispersed nanoparticles were added to dissolved PLLA (in chloroform) to obtain ZnO concentrations ranging from 0.05wt.% to 5wt.%. To obtain a good dispersion of nanoparticles within the polymer, PLLA-ZnO dispersions were submitted to an additional sonication step for 5 minutes before precipitating them in an excess of methanol. This method ensures a homogeneous distribution of nanoparticles (NPs) within the PLLA matrix. Once resulting materials were dried during 48h at 60°C in a vacuum-oven, films with a thickness of  $80\pm 10\mu\text{m}$  were fabricated in a hydraulic hot press by compression moulding at 200°C for 4 minutes under a pressure of 150 MPa.

### Wide angle X-Ray diffraction (WAXD)

Room temperature wide angle X-Ray Diffraction (WAXD) has been conducted in order to elucidate the crystalline structure of ZnO nanoparticles and PLLA/ZnO nanocomposites during their hydrolytic degradation. X-ray powder diffraction patterns were collected in a PHILIPS X'PERT PRO automatic diffractometer in theta-theta configuration, secondary monochromator with Cu-K $\alpha$  radiation ( $\lambda = 1.5418 \text{ \AA}$ ) and a PIXcel solid state detector. The sample was mounted on a zero background silicon wafer fixed in a generic sample holder. Data were collected from 20 to 75° 2 $\theta$  (step size = 0.026) at RT. The presence of oxygen vacancies in the ZnO lattice has been determined by WAXD measurements on a Bruker D8 Advance diffractometer operating at 30 kV and 20 mA, equipped with a Cu tube ( $\lambda = 1.5418 \text{ \AA}$ ), a Vantec-1 PSD detector, and an Anton Parr HTK2000 high-temperature furnace. The powder patterns were recorded in 2  $\theta$  steps of 0.0167° in the  $10 \leq 2\theta \leq 60$  range, counting for 2 s per step (total time 2h). Data sets were recorded at 30, 200, 225 and 250°C with a 0.2 °C s<sup>-1</sup> heating rate.

### Morphological characterization

ZnO nanoparticles have been analyzed by Transmission electron microscopy (TEM). A droplet of diluted ZnO suspension (0.1% (w/w)) in distilled water was deposited on a carbon-coated grid. TEM was carried out using a Philips CM120 Biofilter apparatus with STEM module at an acceleration voltage of 120 kV. Cryofractured surfaces of nanocomposites have been analyzed in a Hitachi S-4800 field emission scanning electron microscope (FE-SEM) at an acceleration voltage of 5 kV. Surfaces were chromium-coated in a Quorum Q150T ES turbo-pumped sputter coater (5 nm thick coating).

### Thermogravimetric analysis (TGA)

Thermodegradative behaviour of nanocomposites was studied by means of Thermal Gravimetric Analysis (TGA METTLER TOLEDO 822e) in alumina pans by heating the samples from room temperature to 500°C at 10°C/min with nitrogen flux of 50 ml/min. Thermodegradation products (exhaust gases upon heating the samples) were analyzed using a Thermo Nicolet Nexus 670 FTIR spectrophotometer connected through an interface to DTG-60 Shimadzu thermobalance. Neat PLLA and its PLLA/ZnO 1wt.% nanocomposite were heated from room temperature to 500°C at 10°C/min under nitrogen atmosphere. FTIR scans were taken every 16s.

### Contact angle measurements

Water was used as the probe liquid for the determination of hydrophobicity at the nanocomposite surface. Measurements were carried out by sessile drop method (2 $\mu\text{L}$  per drop at a rate of 2 $\mu\text{L}/\text{s}$ ) using a Neurtek Instruments OCA 15 EC at room temperature. The average values were calculated using six measurements of each composition.

### Hydrolytic degradation

Neat PLLA and its ZnO nanocomposites (square-shaped; 1cm<sup>2</sup>) were hydrolytically degraded in an oven at 80°C. 80 $\mu\text{m}$  thick samples with a surface area to volume ratio of 0.2cm<sup>-1</sup> were immersed in a PBS solution (PBS tablets dissolved in Milli-Q water; pH=7.4) and they were removed after 1, 3, 6, 10, 12, 18 and 25 days. The pH evolution of the medium has been monitored using a 691 pH Meter (Metrohm).

### Fourier transform infrared spectroscopy (FTIR)

Infrared spectra in transmission KBr mode were recorded on a Thermo Nicolet Nexus 670 FTIR spectrophotometer. Samples were prepared by spreading two drops of a 2wt.% solution over KBr pellets. The solution was dried in vacuum at 60°C for 24h before characterization. Each IR spectrum consisted of 64 scans taken in the range 400–4000cm<sup>-1</sup> with a resolution of 2 cm<sup>-1</sup>. The average values over three replicates are reported for each material.

## Results and discussion

### ZnO nanoparticle characterization

Both X-ray Diffraction (WAXD) and Transmission Electron Microscopy (TEM) have been carried out to determine the structure of ZnO nanoparticles, which affects the physicochemical properties of PLLA/ZnO nanocomposites. As depicted in Fig 1a, WAXD data exhibits featured reflections of hexagonal crystal system of ZnO,

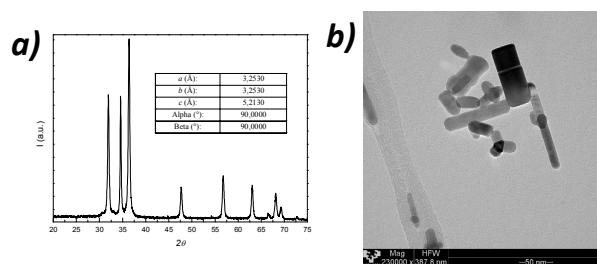


**Fig. 1** WAXD pattern of ZnO nanoparticles (a) and representative transmission electron microscopy (TEM) image showing the hexagonal structure of ZnO nanoparticles at a 230,000x magnification (b).

known as Wurtzite (P63mc space group, with crystal lattice dimensions shown in the insert).<sup>20</sup> TEM micrographs confirm the nanoscale nature of ZnO particles, which present a rod-shaped structure of 15-30nm wide and 25-85nm long.

### Thermal degradation of PLLA and PLLA/ZnO nanocomposites

PLLA is one of the most sensitive thermoplastic to high temperatures in comparison with other polyesters such as poly( $\epsilon$ -caprolactone) (PCL) or poly(L-lactide-co- $\epsilon$ -caprolactone) (PLCL).<sup>21</sup> Fig 2 shows thermogravimetric (a) and weight loss rates (b) of neat PLLA and its ZnO nanocomposites with a concentration up to 5wt.%, being their characteristic thermodegradation temperatures summarized in Table 1. Results show a continuous reduction on the thermal stability because of the catalytic behaviour of ZnO.

As shown in Table 1, thermal degradation of unreinforced polymer begins ( $T_{5wt.}$ ) at 340.2°C and reaches its maximum rate ( $T_{peak}$ ) at 366.8°C. Conversely, PLLA/ZnO 5wt.% nanocomposite begins to degrade almost 100°C below, at 243.4°C, to attain its maximum rate at 282.5°C (note that the char residue increases with NP loading due to the high thermal stability of ZnO). As could be seen in Fig 2b, while the derivative TGA curve (DTG) of neat PLLA

shows a bell-shaped curve (representing a single degradation step), nanocomposites containing 0.1wt.% and 0.2wt.% ZnO present a shoulder in their weight lost rates located at temperatures of 307°C and 294°C respectively. Accordingly, the maximum weight lost rate decreases with increasing ZnO content from 3.48%/°C for neat PLLA to a minimum value of 2.63%/°C for its 0.2wt.% nanocomposite, which reflects slower degradation rate for these compositions. This fact is accompanied by wider curve as denoted by a full width at half maximum (FWHM) of 21.9°C for neat polymer in regard to 30.5°C obtained in the case of 0.2wt.% counterpart. At larger concentrations, both curve-shape and FWHM reach similar values to those obtained for PLLA. It should be noted that the first degradation step in nanocomposites containing low ZnO concentration;<sup>22</sup> i.e. 0.1 and 0.2wt.%, may be related to the thermodegradation of PLLA close to ZnO surfaces, the second stage, achieved at higher temperatures, could be associated with the degradation of PLLA that is far from nanoparticles. This behaviour has been previously found in several processes of polymer-based nanocomposites involving chain mobility, where the presence of nanoparticles results in the development of kinetically different phases (for example, in processes concerning crystallization,<sup>23,24</sup> structural relaxation and mechanical reinforcement).<sup>25,26</sup>

On the contrary, at large nanoparticle concentration, the increased exposition of L-lactide units to ZnO surfaces results in the presence of a single degradation step, in which thermodegradation proceeds even in a narrower temperature-range than in the case of neat PLLA as confirmed by a FWHM of 18.5°C for 5wt.% nanocomposite counterpart with respect to 21.9°C in the case of neat polymer. This remarkable continuous decrease in thermal stability of PLLA with ZnO concentration, especially up to 0.2wt.%, may arise from the fact that metallic nanoparticles such as Fe, Al, Zn and Sn catalyze depolymerization reactions of the matrix, boosting the occurring thermodegradation process.<sup>27-29</sup> Indeed, ZnO nanoparticles coordinate PLLA backbone ester groups, accelerating the unzipping depolymerization reactions as would be further discussed in the following section.<sup>30</sup>

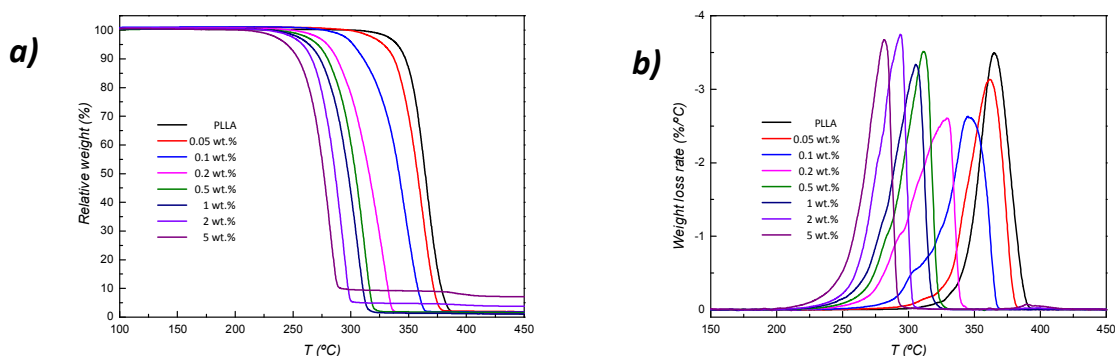


**Fig 2** Thermogravimetric traces (a) and weight lost rates (or derivative TGA curve) (b) of PLLA/ZnO nanocomposites as a function of ZnO concentration.

**Table 1** Characteristic thermodegradation temperatures ( $T_{5\%}$  and  $T_{peak}$ ) and maximum degradation rates ( $\alpha_{max}$ ) of PLLA/ZnO nanocomposites.

ZnO wt.%	0	0.05	0.1	0.2	0.5	1	2	5
$T_{5\%}$ (°C)	340.2	328.3	302.2	279.8	271.1	264	258.2	243.4
$T_{10\%}$ (°C)	347.2	337.8	310.9	288.2	280	273.4	266.2	252.9
$T_{peak}$ (°C)	366.8	363.5	348.2	331.5	312.9	306.7	295.4	282.5
FWHM (°C)	21.9	24	26.3	30.5	21.6	21.9	20.4	18.5

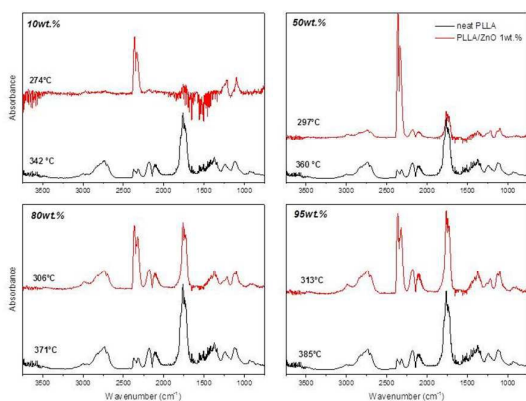


**Fig 3** FTIR spectra of thermodegradation products obtained of neat PLLA and PLLA/ZnO 1wt.% at different weight loss percent: 10, 50, 80 and 95wt.%.

In order to further understand the catalytic effect of ZnO nanoparticles during the heating of PLLA, the resulting degradation products from the PLLA thermodegradation have been analyzed by FTIR. The spectra corresponding to exhaust gases obtained during the thermal degradation of neat PLLA and PLLA/ZnO 1wt.% nanocomposite are shown in Fig 3. It should be pointed out that these spectra correspond to 10, 50, 80 and 95wt.% weight loss of the samples, thus, and according to TGA thermograms shown above, the temperatures at which have been collected differ substantially from each another. The main degradation products obtained during the thermal degradation of neat PLLA ( $(C_3H_4O_2)_n$ ) could be identified as acetaldehyde ( $C_2H_4O$ ;  $2733cm^{-1}$ ,  $1759cm^{-1}$ ,  $1370cm^{-1}$  and  $1106cm^{-1}$  bands), carbon monoxide (CO; two sharp peaks at  $2176cm^{-1}$  and  $2120cm^{-1}$ ), and carbon dioxide ( $CO_2$ ; three absorption bands positioned at  $2362cm^{-1}$ ,  $2334cm^{-1}$  and  $669cm^{-1}$ ). Furthermore, small traces of L-lactic acid ( $C_3H_6O_3$ ; narrow peak at  $1739cm^{-1}$  and a broad band in  $1000-1500cm^{-1}$  range with maximum at  $1457cm^{-1}$ ,  $1212cm^{-1}$ ,  $1128cm^{-1}$  and  $1045cm^{-1}$ ) and low-molecular-weight by-products such as formic acid ( $CH_2O_2$ ; main three bands at  $1700-1820cm^{-1}$ ,  $1050-1130cm^{-1}$  and  $550cm^{-1}-750cm^{-1}$ ) could be observed. The spectra corresponding to the gaseous products evolved from neat PLLA and PLLA ZnO 1wt.% at weight loss of 40% and their assignments are depicted in the Fig 4 (enlarged spectra within the  $1600-2000cm^{-1}$  region is provided in the Supplementary Data, Fig S2). These observations agree with the investigations carried out by MnNeil and Leiper,<sup>31</sup> who found that PLLA chain cleavage produces cyclic oligomers, lactide, acetaldehyde, carbon monoxide and carbon dioxide.

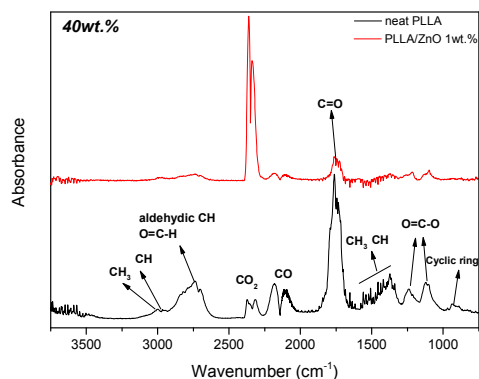
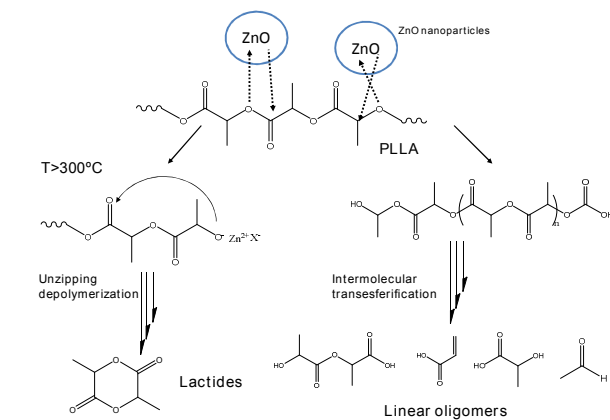


**Fig 4** FTIR spectra of the evolved gases of neat PLLA and PLLA/ZnO 1wt.% at 40wt.%, recorded at 294°C and 357°C, respectively.



**Scheme 1** Expected degradation mechanism in PLLA/ZnO nanocomposites.

Additionally, during the last part of thermodegradation process water is produced as a consequence of L-lactid acid oligomer fragmentation.<sup>32</sup> The results obtained from the analysis of the evolved gases upon thermal decomposition suggest that the degradation of the PLLA/ZnO nanocomposites combines unzipping depolymerization and random transesterification processes. In FTIR spectra of PLLA/ZnO 1 wt.% nanocomposite enlarged for  $1000-2000cm^{-1}$  region (Fig S3) an overlapped presence of aldehyde and L-lactic could be observed. The observation of acetaldehyde and formic acid degradation exhausts corresponds to a transesterification process. Besides, beyond  $300^\circ C$  a characteristic lactide peak is observed at  $940cm^{-1}$  in Fig S3, indicating an unzipping depolymerization reaction. In the Scheme 1 a possible reaction mechanisms for PLLA/ZnO nanocomposites is proposed. These results agree with the previous studies of PLLA/metal oxide composites with MgO, CaO and SnO,<sup>5,6,32,33</sup> in which a catalytic effect of these oxides have been analysed. The degradation of PLLA catalyzed by ZnO nanoparticles present similarities to MgO catalyzed process since lactides are present at higher temperature than  $250^\circ C$  observed for CaO.<sup>5,6</sup> On the other hand, at Sn-catalyzed degradation a random transesterification have been observed.

Although in both PLLA and PLLA/ZnO 1wt.% degradation processes the same products are formed, there are considerable divergences when considering the relative intensity of absorption bands. Indeed, while acetaldehyde, carbon dioxide and carbon monoxide are formed from the beginning of PLLA thermodegradation (Fig 3) and their intensity-ratios remains fairly unchanged over the entire decomposition reaction, thermodegradation products of PLLA/ZnO 1wt.% nanocomposite strongly depends on the conversion rate. Table 2 shows the ratio between evolved acetaldehyde and  $CO_2$  calculated from the intensity ratio between absorption bands located at  $1759cm^{-1}$  and  $2362cm^{-1}$ . In this sense, it can be clearly observed that acetaldehyde represents the main degradation product of neat polymer, while in presence of 1 wt.% of ZnO nanoparticles much larger quantities of CO and  $CO_2$  are evolved during the thermodegradation process. This is in line with the work developed by Saleh et al.,<sup>34</sup> where it has been showed that ZnO generates  $\cdot OH$  radicals that could react with gaseous acetaldehyde ( $CH_3CHO$ ) to generate carbon dioxide and water. From the beginning of the PLLA degradation, acetaldehyde/ $CO_2$  ratio is found to be about 5, which gradually increases up to 10.54 when 70wt.% has been degraded (at  $367^\circ C$ ). Then, an increase of temperature up to  $385^\circ C$  reduces the acetaldehyde/ $CO_2$  ratio to 5.67. At 95wt.% loss mainly formic acid is generated, which is significantly less volatile compound than

**Table 2** Evolved acetaldehyde/CO<sub>2</sub> ratio of neat PLLA and PLLA/ZnO 1wt.% nanocomposite as depending on the mass loss.

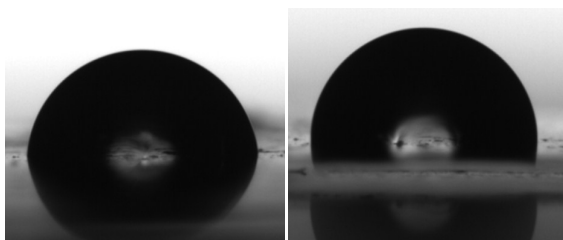
ZnO concentration	Mass loss (wt.%)								
	20	30	40	50	60	70	80	90	95
0 wt.%	5.23	5.78	6.82	9.31	9.79	10.54	10.27	8.91	5.67
1 wt.%	0.08	0.09	0.13	0.21	0.31	0.48	1.06	1.04	0.73

acetaldehyde. On the contrary, as denoted by the increase of the absorption bands located at  $2362\text{cm}^{-1}$  and  $2334\text{cm}^{-1}$ , CO<sub>2</sub> yield dramatically rises in presence of ZnO nanoparticles, being the amount of evolved CO<sub>2</sub> much larger than that of acetaldehyde (acetaldehyde/CO<sub>2</sub> ratio is about 0.08) during the initial stages of thermodegradation, which represents a 65-fold change in comparison with neat polymer.

As shown in Fig S4, concerning to the volatility of compounds it is important to note that, for the same temperature, the vapour pressure of CO<sub>2</sub> is 42753 mm Hg, being the vapour pressure of acetaldehyde 57 times smaller (42753 mm Hg vs. 740 mm Hg).<sup>35</sup> Thus, according to Raoult's law it is reasonable to suppose that the primary reason of the reduced thermal stability of PLLA/ZnO nanocomposites regarding neat PLLA arises from the generation of more volatile thermodegradation products in the presence of ZnO nanoparticles.<sup>36</sup> To the best of our knowledge, this is the first report in which TGA-FTIR measurements show that the presence of nanofillers modifies the thermodegradation products of PLLA. The developed CO and CO<sub>2</sub> gases could be used for active packaging applications since they could effectively extend the self-life of packed foods. Indeed, FDA has approved the use of carbon monoxide as primary packaging system,<sup>37</sup> while carbon dioxide could be used as oxygen scavenger to remove, or at least decrease the amount of oxygen gas into the package.<sup>38</sup> Moreover, it has been proven that CO<sub>2</sub> limits the microbial growth in foods such a fish, cheese and meat.<sup>39</sup> Another interesting application is the development of methanol as an alternative to petro-based fuels since it could be produced by the hydrogenation of both carbon monoxide and carbon dioxide (for example, by using bimetallic Cu-ZnO and Pd-Cu catalysts).<sup>40</sup>

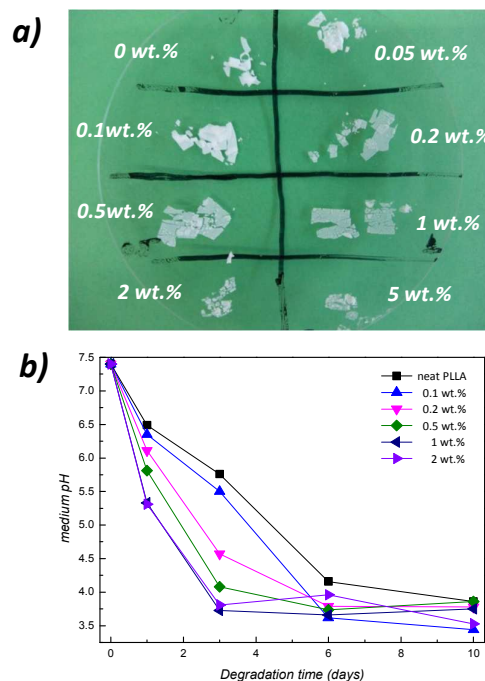
### Surface hydrophobicity

It is well known that the affinity between the sample and the solvent affects the resulting hydrolytic degradation behaviour of materials. In this sense water contact angle (WCA) measurements were carried out to further elucidate the occurring degradation mechanism. As illustrated in Fig 5, an increased surface hydrophobicity with the addition of ZnO from  $81.2\pm 3.9^\circ$  for neat polymer to  $90.8\pm 2.4^\circ$  for 5wt.% nanocomposite has been obtained. This behaviour has been previously reported for different polymer/ZnO nanocomposites.<sup>41</sup>

**Fig 5** Representative images of a water drop at the surface of neat PLLA (left) and 5wt.% nanocomposite film (right).

### Hydrolytic degradation

It is well established that polyesters such as Poly(L-lactide) undergo their hydrolytic degradation through random-scission of ester linkages.<sup>42</sup> Since PLLA could be considered as a heterogeneous material where amorphous and crystalline domains present different molecular mobility,<sup>43,44</sup> in order to avoid the effect introduced by the crystalline phases on the resulting hydrolytic degradation of PLLA/ZnO nanocomposites (crystalline phases present an increased resistance to hydrolytic degradation in regard to amorphous ones),<sup>42</sup> samples with a crystallinity degree around 11-13% (see corresponding Differential Scanning Calorimetry (DSC) traces in Supplementary Data, Fig S5) have been submitted to an accelerated hydrolytic degradation at 80°C in phosphate buffered saline (PBS). Fig 6a shows the physical aspect of PLLA/ZnO nanocomposites once they were removed from PBS solution (after 24h at 80°C) and after being completely dried. It could be observed that nanocomposites containing larger ZnO concentrations undergo physical disintegration to a larger extent than neat PLLA. This fact could be associated with a ZnO-initiated hydrolysis mechanism, in which metallic nanoparticles accelerate the ester-bond hydrolysis of PLLA. To further confirm the catalytic effect of zinc oxide, as shown in Fig 6b, the pH evolution of the medium for a composition range of 0-2wt.% over 10 days of degradation at 80°C has been measured

**Fig 6** Photograph showing physical disintegration of PLLA/ZnO films with concentrations up to 5wt.% after 24h in PBS medium at 80°C (a) and pH evolution of the PBS degradation medium over 10 days at 80°C. Nanocomposites with a concentration up to 2wt.% have been submitted to hydrolytic degradation (b).

(all the nanocomposite films have been immersed with a surface area to volume ratio of  $0.2\text{cm}^{-1}$  at a starting pH of 7.4). Since the pH decrease over the time is due to the release of acidic by-products that have been expelled to the outside medium during the degradation, the determination of the pH of the medium present in Falcon tubes would allow us to determine the extent of hydrolytic degradation. It could be seen that for all the compositions, after 10 days the pH of the medium decreases from 7.4 up to 3.5-3.8, although this decrease progressively occurs at shorter times when increasing nanoparticle content.

For instance, after one day, the pH decreases from 7.4 to 5.6 with the addition of 1wt.% of nanoparticles, while the sample containing neat PLLA present a pH value of 6.5, suggesting that the presence of ZnO accelerates the ester hydrolysis of the PLLA matrix. Moreover, the released acidic products are accumulated in the PBS solution and further autocatalyze the degradation by the generated carboxylic end-groups,<sup>45</sup> speeding up the overall degradation kinetic. For instance, after three days the pH difference of the solution containing neat PLLA and its 1wt.% nanocomposite is even larger than that achieved after one day (1.7 vs. 0.7). After the sixth day, all the nanocomposites have been almost completely diffused into the medium, reaching a nearly constant pH value of 3.5-3.9 depending on the ZnO concentration. As reported by Höglund et al.,<sup>46</sup> oligomers become water-soluble when the molar mass falls below  $1000\text{g/mol}$ , which corresponds to 13 repeating LA units.<sup>47</sup> Resulting lactic acid could be again easily converted into PLLA, closing the loop towards a greener production of biopolymers.

To better understand how this catalytic reaction takes place in PLLA/ZnO nanocomposites, as depicted in Fig 7a, samples have been analyzed by Fourier transform infrared spectroscopy (FTIR). FTIR spectra have been normalized to the characteristic PLLA carbonyl absorption band located at  $1759\text{cm}^{-1}$ . Although they present similar structures, some differences could be observed in their corresponding FTIR spectra. During the hydrolytic degradation of PLLA/ZnO nanocomposites, as a result of the scission of the main chain ester bonds, shorter chains would be found, yielding more carboxylic acid and alcohol groups per mass sample regarding non-degraded sample. Thus, the relative ratio between the ester bonds and end functional groups, i.e., carboxylic acid/alcohol groups, could indicate the extent of the degradation process. Upon degradation the intensity of  $-\text{CH}$  stretching (achieved at  $2997\text{cm}^{-1}$  and  $2945\text{cm}^{-1}$ ) and  $-\text{CO}$  stretching ( $1268\text{cm}^{-1}$ ) absorption bands decrease as ZnO concentration increases, indicating a reduction on the amount of ester bonds.<sup>48,49</sup> A shoulder centred at  $1715\text{cm}^{-1}$  appears in the case of neat PLLA and its 0.05wt.% nanocomposite, which signifies an increased amount of ester groups in comparison with highly filler nanocomposites.<sup>50</sup> In addition, the band centred at  $922\text{cm}^{-1}$ , which corresponds to a combination of  $\text{CH}_3$  rocking mode of PLLA crystals and C-C backbone notably decreases its intensity as ZnO concentration increases,<sup>51</sup> i.e., as degradation further evolves.

As a result of the progressive chain-shortening during hydrolytic degradation, the achieved decrease in molecular entanglement together with increased chain mobility boost the development of highly-ordered crystalline phases.<sup>52</sup> More precisely, wide angle X-ray diffraction patterns of hydrolytically degraded nanocomposites (Fig S6a) denote a progressive increase on the crystalline fraction in regard with amorphous phase as ZnO concentration increases as denoted by a decrease on the amorphous halo at higher ZnO concentrations. Additionally, DSC results (Fig S6b) show lower melting temperature of nanocomposites in presence of zinc oxide together with an increase on the  $X_c$  crystallinity degree from 50.1% for neat polylactide to 69.1% for its 5wt.% nanocomposite. Those

results are in agreement with obtained FTIR spectra and indicate an accelerated chain-scission of polylactide macromolecules in presence of zinc oxide nanoparticles.

Furthermore, it has been previously demonstrated that the carbonyl ( $\text{C}=\text{O}$ ) stretching region of polylactides is highly sensitive to conformational changes.<sup>17,53</sup> Although from a theoretical point of view crystallization should not modify the location of absorption bands, their intensity changes because of the induced changes in refractive index and density by new crystalline regions.<sup>54</sup> Indeed, the increased molecular order in those ordered/semi-ordered domains results in narrower IR bands located at the same wavenumber than the original band.<sup>16</sup> Accordingly, as shown in Fig 7b, the FWHM of the carbonyl band continuously decreases from  $27.7\text{cm}^{-1}$  in the case of neat PLLA to  $13.8\text{cm}^{-1}$  for its PLLA/ZnO 2wt.% nanocomposite counterpart. It is worthy to note that, as occurs with the pH values (see Fig 6b), the main changes are achieved at concentrations up to 1wt.%, suggesting that particle

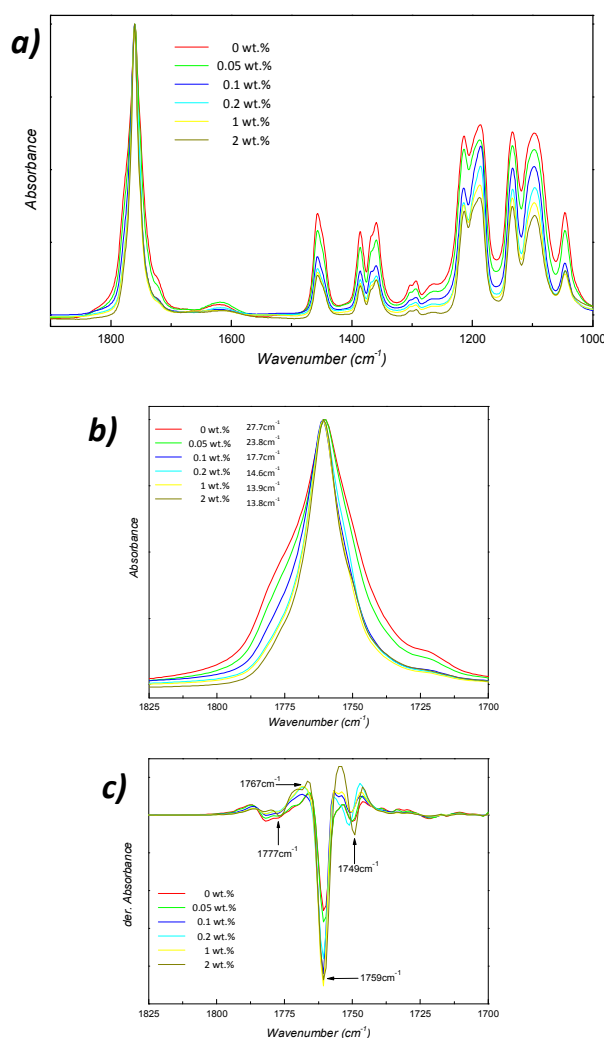


**Fig 7** FTIR spectra of PLLA/ZnO nanocomposites hydrolytically degraded for 24h in PBS medium at  $80^\circ\text{C}$  (a); carbonyl ( $\text{C}=\text{O}$ ) stretching region of hydrolytically degraded PLLA/ZnO nanocomposites (b) and its corresponding second derivative (c). The insert in part a shows obtained FWHM values.

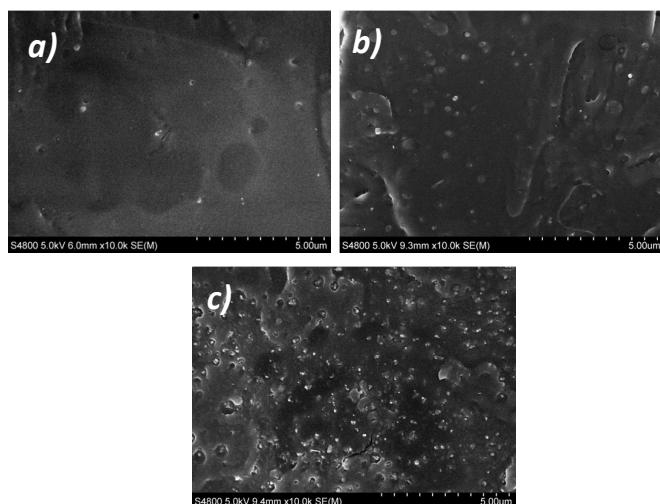


**Fig 8** Representative FE-SEM micrographs showing ZnO dispersion in PLLA matrix for concentrations of 0.5wt.% (a), 1wt.% (b) and 5wt.% (c).

aggregation occurs at larger concentrations than 1wt.%. This fact has been confirmed by FE-SEM micrographs displayed in Fig 8, where it could be observed that concentrations of 0.5-1wt.% ZnO nanoparticles remain well dispersed within the matrix, whilst nanocomposite containing 5wt.% presents large ZnO aggregates.

It is reported that the splitting in the second derivative of the C=O stretching band of PLLA occurs as a result of ordered phases with different chain conformation. As demonstrated in Fig 7c, the second derivative for hydrolytically degraded PLLA/ZnO nanocomposites presents four main components, which arise from the presence of four distinct conformations occurring in PLLA known as gauche-gauche (gg), trans-gauche (tg), gauche-trans (gt) and trans-trans conformers, which absorb respectively at 1777, 1767, 1759 and 1749  $\text{cm}^{-1}$ .<sup>55</sup> It is suggested that the relative areas of those peaks depend on the relative population of the conformers. Thereby, it could be concluded that the fraction concerning to gt conformer (showing a narrow derivative peak) notably increased with the addition of ZnO nanoparticles, together with a decrease in the amount of amorphous gg conformers (absorbance at 1776  $\text{cm}^{-1}$ ).<sup>56</sup> This gt conformer has the lowest energy with a  $10_3$  helical chain conformation,<sup>57</sup> denoting that PLLA/ZnO nanocomposites crystallize into  $\alpha$  crystal form during the hydrolytic degradation. Those data suggest that as ZnO fraction increases, the initially amorphous nanocomposites evolve towards more crystallized materials as a result of the molecular weight reduction. This crystallinity increase ascribed to a molecular weight reduction provides further evidence about the accelerated hydrolytic degradation in presence of ZnO nanoparticles.

We hypothesize that the degradation reactions are initiated by ZnO nanoparticles. In this sense, wide angle X-ray diffraction experiments have been carried out to investigate the structural changes occurring in ZnO nanoparticles during the degradation of nanocomposites. WAXD patterns of PLLA/ZnO 5wt.% nanocomposite upon degradation are shown in Fig 9. The reflections corresponding to ZnO (100), (002) and (101) planes of non-degraded nanocomposite show a shoulder (see Fig S7 for deconvoluted pattern), which has been recently ascribed to the oxygen vacancies present in the lattice.<sup>58,59</sup> During the degradation of nanocomposite this shoulder disappears and diffraction peaks

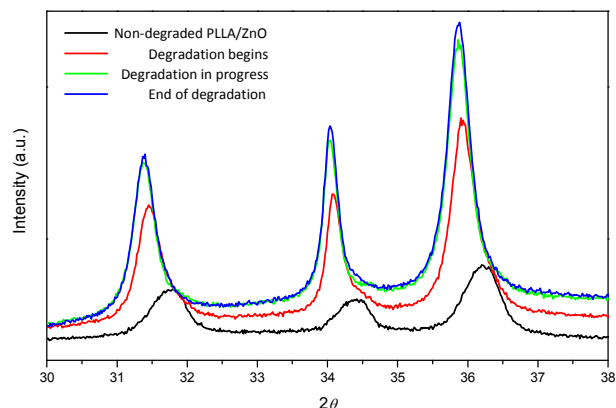


**Fig 9** Wide angle X-ray diffraction patterns of PLLA/ZnO 5wt.% nanocomposite upon degradation.

are continuously shifted towards lower  $2\theta$  angles, denoting a steady increase of the unit cell parameters. This expansion of the unit cell is attributed to a decrease of the residual stress induced by the decrease of oxygen vacancies in the lattice.<sup>60</sup>

In the light of obtained X-ray diffraction and spectroscopic results arising from both thermal and hydrolytic degradation, and taking into account the increased surface hydrophobicity of nanocomposite films, a model concerning the catalytic mechanism in PLLA/ZnO nanocomposites is proposed in Fig 10. In overall, it could be concluded that biopolymer degradation is initiated by zinc oxide nanoparticles. Upon thermodegradation ZnO nanoparticles fill their vacancies with O atoms originating from polylactide macromolecules, leading to unzipping depolymerization and intermolecular transesterification reactions as shown in Scheme 1. On the contrary, hydrolytic degradation proceeds when  $\text{H}_2\text{O}$  is dissociated on oxygen vacancy sites.<sup>61,62</sup> Thus, two hydroxyl groups for each oxygen atom are generated, which initiates the degradation of polymer host by attacking adjacent PLLA chains.

The increased degradation kinetics with ZnO concentration may be explained in terms of polymer/filler interfacial features since the reported catalysis changes are related to the amount of available ZnO surfaces. As zinc oxide concentration raises the formation of

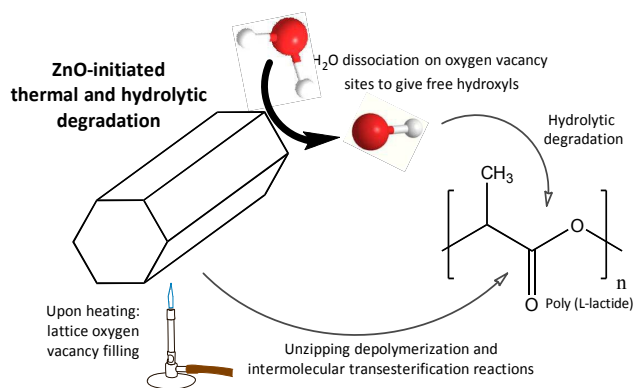


**Fig 10** Schematic representation showing the mechanism of ZnO-initiated degradation.

vats interfacial regions are enough to boost the overall degradation reaction of bulk PLLA because the occurring reactions at ZnO surfaces. Larger concentrations than 0.5-1wt.% result in an increase of direct contacts between adjacent nanoparticles, leading to the formation of bundles that reduce ZnO-PLLA interfacial area per single nanoparticle, which notably limits the catalyzing effect of ZnO.

## Conclusions

In this work PLLA/ZnO nanocomposites with homogeneously dispersed nanoparticles have been prepared. TGA results show that during thermodegradation process of nanocomposites ZnO nanoparticles dramatically lower the thermal degradation temperature by 100°C, being acetaldehyde and CO<sub>2</sub> the main degradation products of neat PLLA and PLLA/ZnO nanocomposites respectively. It is shown that the degradation of the PLLA/ZnO nanocomposites combines unzipping depolymerization and transesterification processes. The accumulation of acidic degradation products in PBS proves that hydrolytic degradation proceeds noticeably faster as ZnO concentration increases. In addition, FTIR spectra demonstrate the presence of shorter polymeric chains when in presence of zinc oxide, with more carboxylic acid groups in comparison to ester groups, suggesting a more marked backbone scission at ester bonds. In addition, according to the splitting in the second derivative of the C=O stretching band, larger crystalline regions are developed as a result of faster hydrolytic degradation as ZnO concentration increases.

WAXD experiments demonstrate that the amounts of oxygen vacancies present in the ZnO lattice are reduced upon degradation. We hypothesize that both thermal and hydrolytic degradation are initiated at ZnO surfaces, leading to unzipping depolymerization/intermolecular transesterification reactions upon thermodegradation or dissociated hydroxyls which initiated the hydrolysis of ester bonds during the hydrolytic degradation. Thereby, the lactic acid resulting from the hydrolytic degradation could be again easily converted into PLLA, closing the loop towards a greener production of biopolymers. It is expected that those findings would open new insights in the use of naturally-available materials as efficient catalyst for the recycling of biopolymers towards the development of eco-friendly disposable polymeric waste.

## Acknowledgements

E.L. thanks the University of the Basque Country (UPV/EHU) for a postdoctoral fellowship. In addition, we gratefully acknowledge Corbion-Purac for the kind donation of PLLA polymer. Authors thank the Basque Country Government for financial support (Ayudas para apoyar las actividades de los grupos de investigación del sistema universitario vasco, IT718-13).

## Notes and references

- 1 R. Auras, B. Harte and S. Selke, *Macromol. Biosci.* 2004, **4**, 835-864.
- 2 R.E. Drumright, P. R. Gruber and D. E. Henton, *Adv. Mater.* 2000, **12**, 1841-1846.

- 3 P. Gruber and M. O'Brien, *Polyactides NatureWorks™ PLA. Biopolymers in 10 Volumes*, Eds., Wiley-VCH, Weinheim 2002.
- 4 X. Helan, and Y. Yang, *Degradable Polymers and Materials: Principles and Practice* (2nd Edition). ACS Symposium Series 2012.
- 5 Y. Fan, H. Nishida, T. Mori, Y. Shirai, T. Endo. *Polymer*, 2004, **45**, 1197-1205.
- 6 T. Motoyama, T. Tsukegi, Y. Shirai, H. Nishida and T. Endo, *Polym. Degrad. Stab.* 2007, **92**, 1350-1358.
- 7 J. Huang, X. Xu, C. Gu, W. Wang, B. Geng, Y. Sun and J. Liu, *Sensors Actuators B: Chem.* 2012, **173**, 599-606.
- 8 A. M. Ali, E. A. C. Emanuelsson and D. A. Patterson, *Appl. Catal. B: Environ.* 2010, **97**, 168-181.
- 9 R. Wahab, S. K. Tripathy, H. S. Shin, M. Mohapatra, J. Musarrat, A. A. Al-Khedhairi and N. K. Kaushik, *Chem. Eng. J.* 2013, **226**, 154-160.
- 10 B. Cheng and E. T. Samulski, *Chem. Commun.* 2004, **227**, 986-987.
- 11 F. Werner, J. F. Gnichwitz, R. Marczak, E. Palomares, W. Peukert, A. Hirsch and D. M. Guldi, *J. Phys. Chem. B* 2010, **114**, 14671-14678.
- 12 E. Lizundia, L. Ruiz-Rubio, J. L. Vilas and L. M. León, *J. Appl. Polym. Sci.* 2015, **132**, 42426.
- 13 M. Mathlouthi, *Food Packaging and Preservation*, Blackie Academic, London 1994.
- 14 Y. Q. Li, S. Y. Fu and Y. W. Mai, *Polymer* 2006, **47**, 2127-2132.
- 15 B. M. Novak, *Adv. Mat.* 1993, **5**, 422-433.
- 16 P. C. Painter, M. Coleman and J. L. Koenig, *Acta Polym.* 1983, **34**, 66.
- 17 E. Meaurio, I. Martinez de Arenaza, E. Lizundia and J. R. Sarasua, *Macromolecules* 2009, **42**, 5717-5727.
- 18 J. C. Colmenares, E. Kuna, S. Jakubiak, J. Michalski and K.J. Kurzydłowski, *Appl. Catal. B: Environ.* 2015, **170-171**, 273-282.
- 19 P. T. Anastas and J. C. Warner, *Green chemistry: Theory and practice*. New York:Oxford University Press 1998.
- 20 H. Schulz, and K. H. Thiemann, *Solid State Commun.* 1979, **32**, 783-785.
- 21 A. Larrañaga and J. R. Sarasua, *Polym. Degrad. Stab.* 2013, **98**, 751-758.
- 22 T. Ozawa, *J. of Therm. Anal. Calorim.* 1970, **2**, 301-324.
- 23 J. Loosa, T. Schimanski, J. Hofman, T. Peijs and P. J. Lemstr, *Polymer* 2001, **42**, 3827-3834.
- 24 A. Dasari, Z. Z. Yu and Y. W. Mai, *Macromolecules* 2007, **40**, 123-130.
- 25 E. Lizundia, J. R. Sarasua, *Macromol. Symp.* 2012, **321-322**, 118-123.
- 26 J. N. Coleman, M. Cadec, K. P. Ryan, A. Fonseca, J. B. Nagy, W. J. Blau and M. S. Ferreira, *Polymer* 2006, **47**, 8556-8561.
- 27 E. Lizundia, J. L. Vilas, L. M. León, *Carbohydr. Polym.* 2015, **123**, 256-265.
- 28 D. Cam and M. Marucci, *Polymer* 1997, **38**, 1879-1884.
- 29 J. Fernandez, A. Etxeberria and J. R. Sarasua, *Polym. Degrad. Stab.* 2013, **98**, 1293-1299.
- 30 H. Abe, N. Takahashi, K. J. Kim, M. Mochizuki and Y. Doi, *Biomacromolecules* 2004, **5**, 1606-1614.
- 31 I. C. McNeill and H. A. Leiper, *Polym. Degrad. Stab.* 1985, **11**, 267-285.
- 32 Poly(lactic acid): Synthesis, structures, properties, processing, and applications (Wiley Series on Polymer Engineering and Technology), ed. R. Auras, L. T. Lim, S. E. M. Selke and H. Tsuji, New Jersey, John Wiley & Sons, Inc., 2010.

- 33 Y. Fan, H. Nishida, Y. Shirai and T. Endo, *Polym. Degrad. Stab.* 2003, **80**, 503-511.
- 34 T. A. Saleh, M. A. Gondal, Q. A. Drmash, Z. H. Yamani, A. Al-Yamani. *Chem. Eng. J.* 2011, **166**, 407-412.
- 35 N. A. Lange and J. A. Dean, *Lange's Handbook of Chemistry*, 10<sup>th</sup> edition. McGraw-Hill, 1967.
- 36 Petrucci, et al. *General Chemistry Principles & Modern Applications*. 9th ed. Upper Saddle River, NJ: Pearson Prentice Hall 2007.
- 37 E. J. Eilert, *Meat Sci.* 2005, **71**, 122-127.
- 38 T. P. Labuza, *Food Technol.* 1996, **50**, 68-71.
- 39 A. Lopez-Rubio, E. Almenar, P. Hernandez-Munoz, J. M. Lagaron, R. Catala and R. R. Gavara, *Food. Rev. Int.* 2004, **20**, 357-387
- 40 X. Jiang, N. Koizumi, X. Guo and C. Song, *Appl. Catal. B: Environ.* 2015, **170-171**, 173-185.
- 41 P. Kanmani and J. W. Rhim, *Carbohydr. Polym.* 2014, **106**, 190-199.
- 42 A. Larrañaga, P. Aldazabal, F. J. Martin, J. R. Sarasua, *Polym. Degrad. Stab.* 2014, **110**, 121-128.
- 43 E. Lizundia, S. Petisco, J. R. Sarasua, *J. Mech. Behav. Biomed. Mater.* 2013, **17**, 242-251.
- 44 J. Del Rio, A. Etxeberria, N. Lopez-Rodriguez, E. Lizundia, J. R. Sarasua, *Macromolecules* 2010, **43**, 4698-4707.
- 45 C. G. Pitt, F. I. Chasalow, Y. M. Hibionada, D. M.; Klimas and A. J. Schindler, *J. Appl. Polym. Sci.* 1981, **26**, 3779-3787.
- 46 A. Höglund, K. Odelius, A. C. Albertsson, *ACS Appl. Mater. Inter.* 2012, **5**, 2788-2793.
- 47 A. Höglund, M. Hakkarainen, U. Edlund and A. C. Albertsson, *Langmuir* 2010, **26**, 378-383.
- 48 J. Coates, *Interpretation of Infrared Spectra, A Practical Approach*. Encyclopedia of Analytical Chemistry. John Wiley & Sons 2006.
- 49 F. Achmad, K. Yamane, S. Quan and T. Kokugan, *Chem. Eng. J.* 2009, **151**, 342-350.
- 50 J. Palacio, V. H. Orozco and B. L. López, *J. Braz. Chem. Soc.* 2011, **22**, 2304-2311.
- 51 J. M. Zhang, H. Tsuji, I. Noda and Y. Ozaki, *Macromolecules* 2004, **37**, 6433-6439.
- 52 Y. Gong, Q. Zhou, C. Gao and J. Shen, *Acta Biomater.* 2007, **3**, 531-540.
- 53 G. Kister, G. Cassanas and M. Vert, *Polymer* 1998, **39**, 267-273.
- 54 R. G. Snyder, M. Maroncelli, H. L. Strauss and V. M. Hallmark, *J. Phys. Chem.* 1986, **90**, 5623-5630.
- 55 E. Meario, E. Zuza, N. Lopez Rodriguez, J. R. Sarasua, *J. Phys Chem. B* 2006, **110**, 5790-5800.
- 56 K. Aou and S. L. Hsu, *Macromolecules* 2006, **39**, 3337-3344.
- 57 J. Zhang, Y. Duan, H. Sato, H. Tsuji, I. Noda, S. Yan and Y. Ozaki, *Macromolecules* 2005, **38**, 8012-8021.
- 58 F. Kayaci, S. Vempati, C. Ozgit-Akgun, N. Biyikli and T. Uyar, *Appl. Catal. B: Environ.* 2014, **156-157**, 173-183.
- 59 F. Kayaci, S. Vempati, I. Donmez, N. Biyikli and T. Uyar, *Nanoscale*, 2014, **17**, 10224-10234.
- 60 S. A. Ansari, M. M. Khan, S. Kalathil, A. N. Khan, J. Lee and M. H. Cho, *Nanoscale* 2013, **5**, 9238-9246.
- 61 H. Noei, H. Qiu, Y. Wang, E. Löffler, C. Wöll and M. Muhler, *Phys. Chem. Chem. Phys.* 2008, **10**, 7092-7097.
- 62 M. Qu, H. Tu, M. Amarante, Y. Q. Song and S. S. Zhu, *J. Appl. Polym. Sci.* 2014, **131**, 40287.

# Graphical Abstract

Schematic representation showing catalytic reaction in Poly (L-lactide)/ZnO nanocomposites

*Erlantz Lizundia, Leire Ruiz-Rubio, José L. Vilas, Luis M. León*

